



Probabilistic framework for assessing maximum structural response based on sensor measurements



Iris Tien ^{a,*}, Matteo Pozzi ^b, Armen Der Kiureghian ^c

^a School of Civil and Environmental Engineering, Georgia Institute of Technology, Atlanta, GA 30332-0355, USA

^b Department of Civil and Environmental Engineering, Carnegie Mellon University, Pittsburgh, PA 15213-3890, USA

^c Department of Civil and Environmental Engineering, University of California, Berkeley, CA 94720-1710, USA

ARTICLE INFO

Article history:

Received 6 March 2015

Received in revised form 23 March 2016

Accepted 31 March 2016

Keywords:

Probabilistic inference and estimation

Extreme value analysis

Dynamic Bayesian Network

Kalman smoother

Seismic loading

Structural health monitoring

ABSTRACT

A probabilistic framework for Bayesian inference combined with extreme values of Gaussian processes is proposed to assess the maximum of the response of an uncertain structure instrumented with sensors and subject to a stochastic load. The framework is applied to the analysis of the inter-story drift of a multi-story shear-type building under seismic hazard using measurements collected by accelerometers. A cascade of two dynamic systems is proposed to model the stochastic ground motion and the response of the structure. We present an approximate analytical solution to estimate the distribution of the maximum response, and verify the accuracy and limitations of this solution against simulation results. Finally, robustness of the proposed framework to system uncertainties, including uncertainties in the structural characteristics, ground characteristics, and input motion parameters, is investigated.

© 2016 Elsevier Ltd. All rights reserved.

1. Introduction

Monitoring of instrumented civil structures and infrastructure is becoming ubiquitous, as sensors continue to decrease in price and increase in capability. Structural health monitoring (SHM) methods have been developed to both improve the data collected through the development of new sensor devices, as well as facilitate how this data is used to learn about the system. The focus of this paper is on the latter, in how we process sensor data to perform inference on the structural response.

Monitoring systems provide real-time measurements on the dynamic response of structures during extreme events. Information about the structural model and the stochastic load can be integrated into the data processing to probabilistically evaluate features relevant to the post-event condition assessment, such as extreme values of key structural responses.

To do this task, in this paper we propose a framework based on the Kalman smoother for Gaussian linear systems and extreme value analysis of Gaussian processes. The objective is to accurately assess the maximum of the response of a linear structure under stochastic excitation by processing noisy sensor measurements. We apply the framework to the estimation of the inter-story drift

of a multi-story, shear-type building under seismic hazard using information from measurements of accelerometers placed at selected floors of the building. We develop a cascade of two systems, modeling the seismic ground motion and the vibrating structure. We derive an analytical solution to estimate the distribution of the peak response, conditioned on the measurements, and results from this solution are compared with those obtained from Monte Carlo simulations. Finally, we show the proposed probabilistic framework to be robust to system uncertainties, including uncertainties in the structural characteristics, ground characteristics, and input motion parameters. This work informs decision making in the management of structures subject to seismic hazard and for the development and design of smart SHM systems.

2. Background and related work

For Gaussian linear models, the Kalman Filter (KF) [1] and Kalman Smoother (KS) [2] can be used to estimate the system state for dynamically evolving systems by processing sparse measures of the system response. While the KF algorithm computes the posterior probability of the system given past and present measurements, the KS algorithm allows, after an event, to compute the posterior distribution with respect to all measurements collected even after the time at which the state is being evaluated. The KF and KS allow computation of not only the marginal probability of

* Corresponding author at: School of Civil and Environmental Engineering, Georgia Institute of Technology, 790 Atlantic Drive, Atlanta, GA 30332-0355, USA.

E-mail address: itien@ce.gatech.edu (I. Tien).

system state at each time, but also to sample trajectories. The reader is referred to the texts [3,4] for treatment of the KF and KS models.

As the KF and KS perform probabilistic analysis of a dynamic system, they are ideal for structural health monitoring (SHM) applications, where observations of a structure are used to characterize and assess the state of the structure over time. In this study, we are interested in performing inference on the dynamically evolving response of a structure when it is subjected to a stochastic excitation, e.g., an earthquake, based on uncertain information, e.g., sensor measurements.

KF and KS are algorithms for linear Gaussian models, which can be seen as special cases of the Dynamic Bayesian Network (DBN). The DBN is a probabilistic framework that models the evolution of a system or process over time. It consists of a sequence of connected Bayesian Networks (BNs), each representing the system at a time slice t [5]. The evolution in time is represented by directed links between nodes of successive time-slice BNs that carry information on temporal dependencies of the respective processes. Inference on the DBN for linear Gaussian systems can be performed using the KF and KS.

2.1. Probabilistic frameworks for structural health monitoring

Applications of the KF in SHM can be found in [6–8]. In these works, the Extended KF is used for system identification of linear and nonlinear systems. Studies using Bayesian methods in SHM have focused on identifying modal parameters of a structure and performing damage detection. A Bayesian framework to obtain distributions of the modal parameters, including the most probable values of the parameters and their uncertainties, is proposed in [9]. Au et al. [10] and Katafygiotis and Yuen [11] used data from ambient vibrations for modal identification. A Bayesian approach is proposed in [12] to account for uncertainties in the structural system to determine the existence and location of damage. Vanik et al. [13] used the proposed approach to continually update the stiffness parameters of a structure with a high likelihood of reduction in stiffness at a particular location used as a proxy for damage at that location. Rather than damage detection, we are interested in performing inference on the state of a structural system as it is subjected to a specific stochastic hazard.

For the monitoring of structures during extreme events, SHM systems are proposed in [14,15]. These studies are focused on the hardware aspects of the system rather than on performing probabilistic analysis of the data collected using these systems. Wu and Beck [16] used a Bayesian framework and expanded their analysis to the monitoring of a system both before and after an earthquake, with pre-event prognosis and post-event diagnosis. The response of the structure during the seismic event, however, is not analyzed. In general, previous studies using Bayesian methods for SHM limit the use of the Bayes rule to the standard Bayesian updating of system parameters. In this paper, we present a probabilistic framework to estimate the evolution of the structural response to stochastic excitation based on sensor measurements, and show the methodology to be robust to system uncertainties in performing this inference.

3. Method

3.1. System formulation

In the following, a capital bold letter denotes a matrix, such as the mass matrix \mathbf{M} , a small bold letter denotes a vector, as in the vector of structural displacements relative to the ground $\mathbf{u}_s(t)$, and a small italic letter denotes a scalar quantity, such as the

ground displacement $u_g(t)$. Displacement and acceleration are denoted u and a , respectively, while $\mathbf{z}(t)$ collects displacement and velocity values. Subscripts g and s indicate quantities for the ground and structure, respectively.

We model the dynamical system as a cascaded system of two sub-systems: a ground sub-system and a structural sub-system, as shown in Fig. 1.

The ground dynamical sub-system takes a modulated white-noise input $w(t)$, representing the motion at the bedrock, and outputs the acceleration $a_g(t)$ on the ground surface. The structural dynamical sub-system takes $a_g(t)$ as well as ambient noise as excitation and produces the structural response $\mathbf{u}_s(t)$, the vector of nodal displacements relative to the ground. Our interest lies not only in inferring the instantaneous values of $\mathbf{u}_s(t)$ and related responses, but also in their peak values over time. This study assumes linear structural behavior as well as Gaussianity of both the earthquake and ambient-vibration input excitations to allow the use of Gaussian models and the KF described in the following sections. The proposed method can be extended to analyze nonlinear structural behavior by relaxing the assumption of a linear Gaussian system. As such, the current study is appropriate for operating-basis seismic events.

3.1.1. Ground dynamical sub-system

The equation describing the motion on the ground surface relative to the bedrock is given by

$$\ddot{u}_g + 2\zeta_g\omega_g\dot{u}_g + \omega_g^2u_g = -w \quad (1)$$

where ω_g and ζ_g define the angular frequency and damping ratio of the ground filter and w denotes the modulated white-noise acceleration at the bedrock. Written in first-order form with $\mathbf{z}_g = [u_g \ \dot{u}_g]^T$, (1) becomes

$$\dot{\mathbf{z}}_g = \begin{bmatrix} 0 & 1 \\ -\omega_g^2 & -2\zeta_g\omega_g \end{bmatrix} \mathbf{z}_g + \begin{bmatrix} 0 \\ -1 \end{bmatrix} w \quad (2)$$

The total acceleration at the surface of the ground, a_g , is obtained as

$$a_g = \ddot{u}_g + w = [0 \ 1] \dot{\mathbf{z}}_g + w = [-\omega_g^2 \ -2\zeta_g\omega_g] \mathbf{z}_g \quad (3)$$

3.1.2. Structural dynamical sub-system

The equation of motion for a linear structure subjected to base motion is

$$\mathbf{M}\ddot{\mathbf{u}}_s + \mathbf{C}\dot{\mathbf{u}}_s + \mathbf{K}\mathbf{u}_s = -\mathbf{M}\mathbf{i}a_g + \mathbf{f} \quad (4)$$

where \mathbf{M} , \mathbf{C} , and \mathbf{K} denote the mass, damping, and stiffness matrices, respectively, \mathbf{i} is the influence vector relating the degrees of freedom to a unit base motion, and \mathbf{f} models a random external force vector representing the effect of ambient noise, adding uncertainty to the system response. In first-order form, using $\mathbf{z}_s^T = [\mathbf{u}_s^T \ \dot{\mathbf{u}}_s^T]$, (4) becomes

$$\dot{\mathbf{z}}_s = \begin{bmatrix} \mathbf{0} & \mathbf{I} \\ -\mathbf{M}^{-1}\mathbf{K} & -\mathbf{M}^{-1}\mathbf{C} \end{bmatrix} \mathbf{z}_s + \begin{bmatrix} \mathbf{0} \\ -\mathbf{i} \end{bmatrix} a_g + \begin{bmatrix} \mathbf{0} \\ \mathbf{M}^{-1} \end{bmatrix} \mathbf{f} \quad (5)$$

3.1.3. State-space representation

Combining (2), (3) and (5), we obtain a representation of the full dynamical system in first-order form

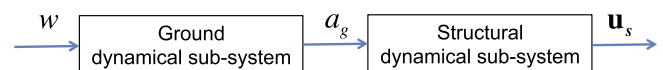


Fig. 1. Dynamical system model, consisting of ground and structural sub-systems.

$$\dot{\mathbf{z}} = \begin{bmatrix} 0 & 1 & \mathbf{0} & \mathbf{0} \\ -\omega_g^2 & -2\zeta_g\omega_g & \mathbf{0} & \mathbf{0} \\ \mathbf{0} & \mathbf{0} & \mathbf{0} & \mathbf{I} \\ \mathbf{i}\omega_g^2 & \mathbf{i}2\zeta_g\omega_g & -\mathbf{M}^{-1}\mathbf{K} & -\mathbf{M}^{-1}\mathbf{C} \end{bmatrix} \mathbf{z} + \begin{bmatrix} 0 \\ -1 \\ \mathbf{0} \\ \mathbf{0} \end{bmatrix} w + \begin{bmatrix} \mathbf{0} \\ \mathbf{0} \\ \mathbf{0} \\ \mathbf{M}^{-1} \end{bmatrix} \mathbf{f} \quad (6)$$

where $\mathbf{z}^T = [\mathbf{z}_g^T \ \mathbf{z}_s^T]$. Consistent with previous studies [17], we define the matrices \mathbf{A}_c and \mathbf{B}_c and vector \mathbf{b}_c so that (6) takes the form $\dot{\mathbf{z}} = \mathbf{A}_c\mathbf{z} + \mathbf{b}_c w + \mathbf{B}_c\mathbf{f}$. Discretizing in time domain in the state-space framework with time step Δt requires the standard transformations $\mathbf{A} = e^{\mathbf{A}_c\Delta t}$, $\mathbf{b} = \mathbf{A}_c^{-1}(\mathbf{A} - \mathbf{I})\mathbf{b}_c$, and $\mathbf{B} = \mathbf{A}_c^{-1}(\mathbf{A} - \mathbf{I})\mathbf{B}_c$ [18]. This leads to

$$\mathbf{z}_{k+1} = \mathbf{A}\mathbf{z}_k + \mathbf{b}w_k + \mathbf{B}\mathbf{f}_k \quad (7)$$

as the full equation of motion for the system in discrete time step k .

3.1.4. Modeling the excitation

To represent the non-stationarity of the ground motion, we model the acceleration at the bedrock as a modulated, band-limited white-noise process. Thus, $w(t)$ is normally distributed with zero mean and a time-varying variance $\sigma_w^2(t)$ with a gamma modulating function, so named because its shape is taken to be proportional to a gamma probability density function (PDF). The gamma PDF is a reasonable model for this purpose, since it is non-negative, starts at and tends to zero, and the shape is skewed with a longer right tail, which is typical of earthquake ground motions. The parameters of the modulating function are determined in terms of descriptive variables of the seismic event. Specifically, we take the mode of the distribution to coincide with the time of the maximum intensity of the ground motion, t_{eq}^{max} , and the middle 90% of the distribution to represent the effective duration of the earthquake motion, D_{5-95} , which we define as the time between 5% and 95% Arias intensity values. These modeling assumptions lead to the shape and scale parameters of the modulating function and the corresponding gamma PDF as $k = \frac{t_{eq}^{max}}{\theta} + 1$ and $\theta = -\frac{1}{2}t_{eq}^{max} + \frac{1}{4}\sqrt{4(t_{eq}^{max})^2 + D_{5-95}^2}$, respectively. The modulating function is scaled by a factor to achieve the desired intensity of the motion. We note that these parameters can be highly uncertain. One approach is to use mean values of the parameters for given earthquake and site characteristics, as described in [19]. Alternatively, these values can be tuned post-event to match the parameters of an observed excitation, where an estimation of the response based on sensor information recorded through the duration of the event is desired. Ideally, these parameters should be estimated from observations of the structural response. However, that would necessitate a costly simulation approach. Hence, as a first attempt at solving this problem, for now we assume these parameters are known. Later, we investigate the robustness of the proposed method to uncertainties in the input ground motion parameters. Fig. 2 shows an example simulation of $w(t)$ with $t_{eq}^{max} = 20$ s, $D_{5-95} = 25$ s, a scale factor of 200, and a discretization time step of $\Delta t = 0.01$ s, which implies a cut-off frequency of 50 Hz [20]. This results in a root-mean-square of the ground acceleration, calculated over the duration of the response [0, 50 s], of 0.64 m/s² and a maximum standard deviation of $\sigma_w(t_{eq}^{max}) = 3.64$ m/s².

3.1.5. System evolution

Given the state-space representation of the system, the system evolution from time step k to $k + 1$ is described by (7). We take \mathbf{f}_k to be normally distributed with zero mean and covariance matrix $\sigma_f^2\mathbf{I}$, where \mathbf{I} is the identity matrix. Further, we assume the force values at different time steps are statistically independent of each

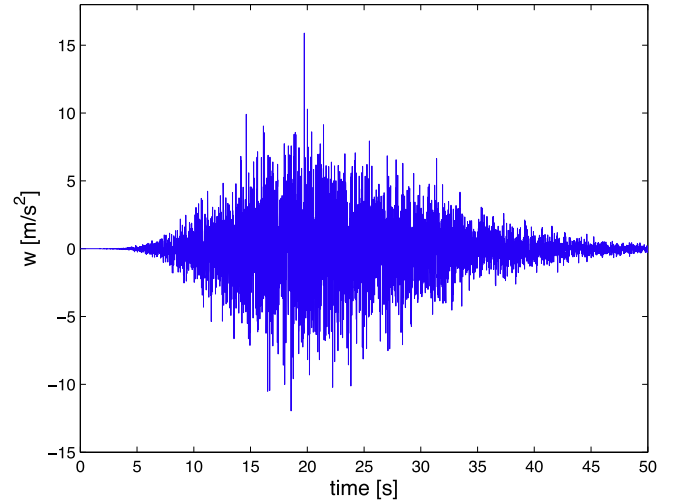


Fig. 2. Bedrock excitation w with time-varying variance $\sigma_w^2(t)$ with gamma modulating function proportional to the gamma PDF.

other and of the ground motion and initial conditions. Including this additional force increases the uncertainty in our model.

3.1.6. Observation equation

We assume sensors mounted on the structure measure the total accelerations,

$$\mathbf{a}_t = \ddot{\mathbf{u}}_s + \mathbf{i}a_g \quad (8)$$

From (4) and \mathbf{z} as defined in (6), we obtain

$$\mathbf{a}_t = -\mathbf{M}^{-1}\mathbf{K}\mathbf{u}_s - \mathbf{M}^{-1}\mathbf{C}\dot{\mathbf{u}}_s + \mathbf{M}^{-1}\mathbf{f} = -\mathbf{M}^{-1}[\mathbf{0} \ \mathbf{0} \ \mathbf{K} \ \mathbf{C}]\mathbf{z} + \mathbf{M}^{-1}\mathbf{f} \quad (9)$$

Let \mathbf{S} define a matrix that selects the degrees of freedom, where accelerometers are placed. The observation equation at each time step k is then given by

$$\mathbf{y}_k = \mathbf{D}\mathbf{z}_k + \mathbf{v}_k + \mathbf{S}\mathbf{M}^{-1}\mathbf{f}_k \quad (10)$$

where $\mathbf{D} = -\mathbf{S}\mathbf{M}^{-1}[\mathbf{0} \ \mathbf{0} \ \mathbf{K} \ \mathbf{C}]$ is the observation matrix and \mathbf{v}_k denotes the vector of measurement errors. We take the measurement errors \mathbf{v}_k to be normally distributed with zero mean and time-independent common variances σ_v^2 , and assume errors at different times and different locations are independent. The objective is to use the sensor measurements \mathbf{y}_k to infer the response of the structure as it evolves with time under seismic excitation.

3.2. DBN representation of the system

With a stochastic excitation, a dynamically evolving structural response, and uncertainties in the system, including uncertainties in sensor measurements, the system to be analyzed is well modeled graphically as a DBN, as shown in Fig. 3.

The DBN consists of a sequence of BNs, each representing the system at a slice in time. Subscript k , $k = 0, 1, \dots, n$, refers to the time step with $k = 0$ indicating initial values, which are also uncertain. The DBN shows the evolution of the system state \mathbf{z} over time, depending on the random processes w and \mathbf{f} , which act as inputs for the system dynamics. The measurements \mathbf{y} are then taken from \mathbf{z} with measurement error \mathbf{v} . Measurements are shaded to indicate that their values are observed.

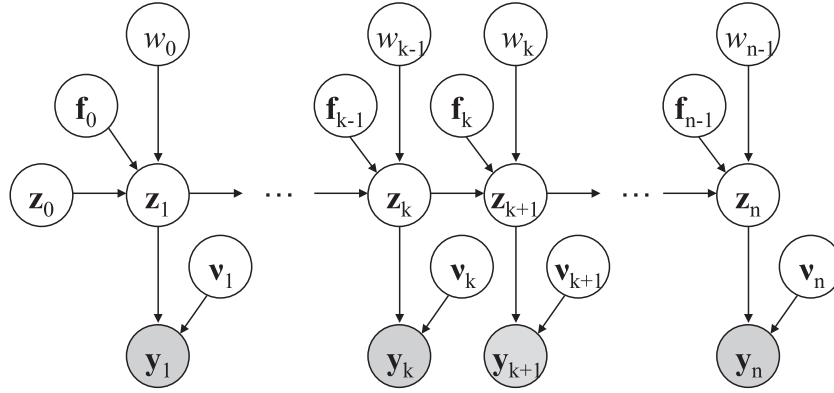


Fig. 3. Representation of the system as a DBN.

3.3. Kalman filter and Kalman smoother

Since we are dealing with a linear Gaussian model, inference on the DBN can be performed by the KF and KS algorithms [21–25]. In this section, we follow the scheme reported in [5]. In addition, we assume observability of the system, so that it is possible to infer the internal behavior of the system based on its outputs [26]. Specifically, our objective is to estimate the state of the system \mathbf{z} given measurements \mathbf{y} . From (7), we predict the mean vector and covariance matrix of the system state at step k as

$$\boldsymbol{\mu}_{\mathbf{z}_k}^p = \mathbf{A}\boldsymbol{\mu}_{\mathbf{z}_{k-1}} \quad (11)$$

$$\boldsymbol{\Sigma}_{\mathbf{z}_k \mathbf{z}_k}^p = \mathbf{A}\boldsymbol{\Sigma}_{\mathbf{z}_{k-1} \mathbf{z}_{k-1}}\mathbf{A}^T + \boldsymbol{\Sigma}_{\mathbf{E}_k} \quad (12)$$

where $\boldsymbol{\Sigma}_{\mathbf{E}_k} = \mathbf{b}\sigma_{w_k}^2\mathbf{b}^T + \boldsymbol{\Sigma}_g^2$ and the superscript P denotes the predicted value. We then calculate

$$\mathbf{e}_k = \mathbf{y}_k - \mathbf{D}\boldsymbol{\mu}_{\mathbf{z}_k}^p \quad (13)$$

$$\mathbf{R}_k = \mathbf{D}\boldsymbol{\Sigma}_{\mathbf{z}_k \mathbf{z}_k}^p\mathbf{D}^T + \sigma_v^2\mathbf{I} \quad (14)$$

$$\mathbf{K}_{G_k} = \boldsymbol{\Sigma}_{\mathbf{z}_k \mathbf{z}_k}^p\mathbf{D}^T\mathbf{R}_k^{-1} \quad (15)$$

In the KF terminology, \mathbf{e}_k is the innovation, \mathbf{R}_k characterizes the uncertainty due to the measurement error, and \mathbf{K}_{G_k} is the Kalman gain matrix [27]. The innovation measures the difference between the measurements and the predicted mean values. The Kalman gain takes into account the accuracy of the observations to provide a weight on the information from the measurements compared to the values from the prediction in updating the estimates. Thus, the estimates of the mean vector and covariance matrix are updated as

$$\boldsymbol{\mu}_{\mathbf{z}_k} = \boldsymbol{\mu}_{\mathbf{z}_k}^p + \mathbf{K}_{G_k}\mathbf{e}_k \quad (16)$$

$$\boldsymbol{\Sigma}_{\mathbf{z}_k \mathbf{z}_k} = (\mathbf{I} - \mathbf{K}_{G_k}\mathbf{D})\boldsymbol{\Sigma}_{\mathbf{z}_k \mathbf{z}_k}^p \quad (17)$$

The KF performs a forward pass through the data to update the estimates of the system state as information from measurements becomes available. The mean and covariance matrix (16) and (17) define the parameters of the posterior normal distribution of state \mathbf{z}_k , given observations $\{\mathbf{y}_1, \dots, \mathbf{y}_k\}$. Once we have information over a fixed time interval, we can perform a backward pass through the data to further update our estimates using the KS [28], thus obtaining the parameters of the posterior distribution given all the observations $\{\mathbf{y}_1, \dots, \mathbf{y}_n\}$. To apply the KS, we first compute the smoother gain matrix

$$\mathbf{J}_k = \boldsymbol{\Sigma}_{\mathbf{z}_k \mathbf{z}_k}\mathbf{A}^T(\boldsymbol{\Sigma}_{\mathbf{z}_{k+1} \mathbf{z}_{k+1}}^p)^{-1} \quad (18)$$

and then update our estimates according to

$$\boldsymbol{\mu}_{\mathbf{z}_k}^{KS} = \boldsymbol{\mu}_{\mathbf{z}_k} + \mathbf{J}_k(\boldsymbol{\mu}_{\mathbf{z}_{k+1}}^{KS} - \boldsymbol{\mu}_{\mathbf{z}_{k+1}}^p) \quad (19)$$

$$\boldsymbol{\Sigma}_{\mathbf{z}_k \mathbf{z}_k}^{KS} = \boldsymbol{\Sigma}_{\mathbf{z}_k \mathbf{z}_k} + \mathbf{J}_k(\boldsymbol{\Sigma}_{\mathbf{z}_{k+1} \mathbf{z}_{k+1}}^{KS} - \boldsymbol{\Sigma}_{\mathbf{z}_{k+1} \mathbf{z}_{k+1}}^p)\mathbf{J}_k^T \quad (20)$$

It is these final estimates of the system state from applying the KS that we use to probabilistically assess the response of the system under the stochastic loads.

The displacement and velocity of any set of degrees of freedom in the structure, or any linear combination of them, at any time step, are modelled as a joint normal distribution, and the algorithms described above allow for computing the corresponding parameters. This description is sufficient for applying the extreme value analysis, as described in the next section. It is noted that the system state trajectories can be easily sampled from the DBN in Fig. 3 by using the Forward Filtering Backward Sampling approach described in [29]. We use samples generated by this method to validate the formulas proposed in the next section.

4. Analytical solution for extreme values of inferred structural response

In reliability analysis, it is often the distribution of extreme values that is critical. Therefore, in this section, we show how the outcome of the probabilistic inference presented above can be used to compute the distribution of the maximum structural response over the duration of the seismic excitation. The objective is, for example, to compute the probability that a critical response quantity will exceed a safe threshold. For this purpose, we derive an approximate analytical solution for the probability of a non-zero-mean, non-stationary process exceeding a specified threshold.

Specifically, we are interested in the probability of the non-stationary process $Z(t)$ exceeding a given threshold ζ during an interval $(0, T)$, where $Z(t)$ is a linear function of the system state \mathbf{z}_s defined previously, and T is the duration of the response. In what follows, we assume $Z(t)$ is a mean-square differentiable process.

Define $Z_{\max} = \max_t Z(t)$ and let $v(\zeta^+, t)$ denote the mean rate of crossing of $Z(t)$ above the threshold ζ at time t . Assuming these crossings constitute Poisson events, the probability of interest is given by [30].

$$\Pr(Z_{\max} > \zeta) = 1 - \Pr(Z_{\max} \leq \zeta) \cong 1 - \exp\left[-\int_0^T v(\zeta^+, t)dt\right] \quad (21)$$

where the approximation is due to the assumption of Poisson crossings and is valid for high thresholds. Due to conditioning on measured responses, $Z(t)$ is not a zero-mean process. Indeed, the mean of $Z(t)$ varies with time. Thus, to obtain $v(\zeta^+, t)$, we cannot

use the well-known formula for up-crossings of a Gaussian process with a constant mean [31]. Define $X(t) = Z(t) - \mu_Z(t)$, where $X(t)$ is now a zero-mean process with $\sigma_X(t) = \sigma_Z(t)$. The up-crossings of the non-zero-mean process $Z(t)$ above a fixed threshold ζ are identical to the up-crossings of the zero-mean process $X(t)$ above a time-varying threshold $\eta(t) = \zeta - \mu_Z(t)$. Therefore, our goal of assessing the probability that random variable $Z(t)$ up-crosses a threshold ζ is equivalent to assessing the probability that random variable $X(t)$ up-crosses a threshold $\eta(t)$. Consider the sketch shown in Fig. 4. We are interested in deriving the mean up-crossing rate of $X(t)$ above the time-varying threshold $\eta(t)$.

We see in Fig. 4 that during the small time interval $(t, t + \Delta t]$, the probability of encountering an up-crossing of level $\eta(t)$ is

$$\begin{aligned} & \Pr\{X(t) < \eta(t)\} \cap \{\dot{\eta}(t) < \dot{X}(t)\} \cap \{\eta(t) + \dot{\eta}(t)\Delta t < X(t) + \dot{X}(t)\Delta t\} \\ &= \Pr\{[\eta(t) + (\dot{\eta}(t) - \dot{X}(t))\Delta t < X(t) < \eta(t)] \cap \{\dot{\eta}(t) < \dot{X}(t)\}\} \\ &= \int_{\eta}^{\infty} \int_{\eta+(\dot{\eta}-\dot{x})\Delta t}^{\eta} f_{X\dot{X}}(x, \dot{x}, t) dx d\dot{x} \\ &= \Delta t \int_{\dot{\eta}}^{\infty} (\dot{x} - \dot{\eta}) f_{X\dot{X}}(\eta, \dot{x}, t) d\dot{x} \end{aligned} \quad (22)$$

where $f_{X\dot{X}}(x, \dot{x}, t)$ is the joint PDF of $X(t)$ and $\dot{X}(t)$ and use has been made of the mean-value theorem for small Δt to arrive at the last expression. Since in a small interval, the probability of more than one up-crossing is negligible compared to that of zero or one crossing, $v(\zeta^+, t)$ is equal to the above probability divided by Δt , i.e.,

$$v(\zeta^+, t) = v_X(\eta(t)^+, t) = \int_{\dot{\eta}}^{\infty} (\dot{x} - \dot{\eta}) f_{X\dot{X}}(\eta, \dot{x}, t) d\dot{x} \quad (23)$$

In our case the distribution $f_{X\dot{X}}(x, \dot{x}, t)$ is jointly normal so that

$$\begin{aligned} f_{X\dot{X}}(\eta, \dot{x}, t) &= \frac{1}{2\pi\sigma_X\sigma_{\dot{X}}\sqrt{1-\rho^2}} \\ &\times \exp\left[-\frac{1}{2(1-\rho^2)}\left(\frac{\eta^2}{\sigma_X^2} - 2\rho\frac{\eta\dot{x}}{\sigma_X\sigma_{\dot{X}}} + \frac{\dot{x}^2}{\sigma_{\dot{X}}^2}\right)\right] \end{aligned} \quad (24)$$

wherein $\eta(t)$, $\sigma_X(t)$, $\sigma_{\dot{X}}(t)$ and $\rho(t) = \rho_{\dot{X}(t)X(t)}$ are all functions of time. Using (24) in (23), after some algebra, we have

$$\begin{aligned} v_X(\eta(t)^+, t) &= \frac{\exp\left[-\frac{1}{2}\frac{\eta^2}{\sigma_X^2}\right]}{2\pi\sigma_X\sigma_{\dot{X}}\sqrt{1-\rho^2}} \left\{ \sigma_{\dot{X}}^2(1-\rho^2) \exp\left[-\frac{r^2}{2\sigma_X^2(1-\rho^2)}\right] \right. \\ &\quad \left. + \sqrt{2\pi(1-\rho^2)}\sigma_{\dot{X}} \left[1 - \Phi\left(\frac{r}{\sigma_X\sqrt{1-\rho^2}}\right)\right] \left(\frac{\sigma_{\dot{X}}\rho\eta}{\sigma_X} - \dot{\eta}\right) \right\} \end{aligned} \quad (25)$$

where $r = \dot{\eta} - \frac{\rho\eta\sigma_{\dot{X}}}{\sigma_X}$ and $\Phi(\cdot)$ indicates the standard normal CDF. The values $\sigma_X(t)$, $\sigma_{\dot{X}}(t)$ and $\rho(t) = \rho_{\dot{X}(t)X(t)}$ are outputs from the inference procedure. At any time step, v_X is computed using (25) and the integral in (21) is approximated by the sum along all steps.

While the KF and KS provide estimates of the evolution of the structural response over time, the solution presented in this section gives us the ability to analytically estimate the probability of the structural response exceeding a given threshold over the duration of the excitation, a probability that cannot be estimated directly from KF or KS. With the expressions given in (21) and (25), this is done analyzing the result of the KS inference. In addition, the analytical solution provides us with results for small exceedance probabilities for which sampling methods, e.g., Monte Carlo simulations, would be infeasible.

5. Numerical application

We apply the proposed method to a 10-story, shear-type building, as shown in Fig. 5. The building is of nominally uniform mass

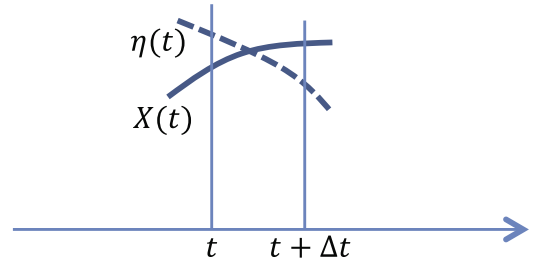


Fig. 4. Up-crossing of a non-stationary zero-mean process above a time-varying threshold.

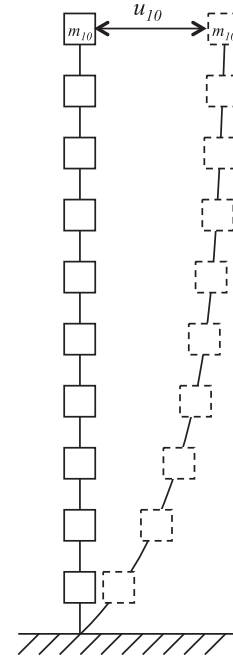


Fig. 5. 10-Story shear-type building model.

and stiffness with these parameter values set such that the nominal fundamental period is 1 s. We assume the building is classically damped with nominal damping ratios being 0.05 in each mode. The parameters of the ground filter are set at $\omega_g/2\pi = 1.5$ Hz and $\xi_g = 0.4$. We take the stochastic excitation at the bedrock level as described for the example realization in Fig. 2, with earthquake parameters $t_{eq}^{max} = 20$ s and $D_{5-95} = 25$ s. The estimated mean peak ground acceleration is roughly 1.6 m/s^2 , obtained by multiplying the peak root mean square of the ground acceleration by a peak factor of 2.5.

We use simulation to investigate the accuracy of the proposed method. For this purpose, we first simulate a seismic event as well as the ambient noise. We compute the structural response from this generated combined excitation, and we call this the “actual” response. We then simulate measurements of this response by adding a randomly generated measurement noise. These represent the observations of floor accelerations that we obtain from the accelerometers mounted on the structure. Then, assuming we have only these noisy measurements of floor accelerations and the system and ground motion parameters, we use our formulation of the system to estimate the response of the structure to the stochastic seismic loading.

The proposed formulation enables us to perform probabilistic inference on any selected response of the structure that can be expressed as a linear function of \mathbf{z}_s . For the present example, we

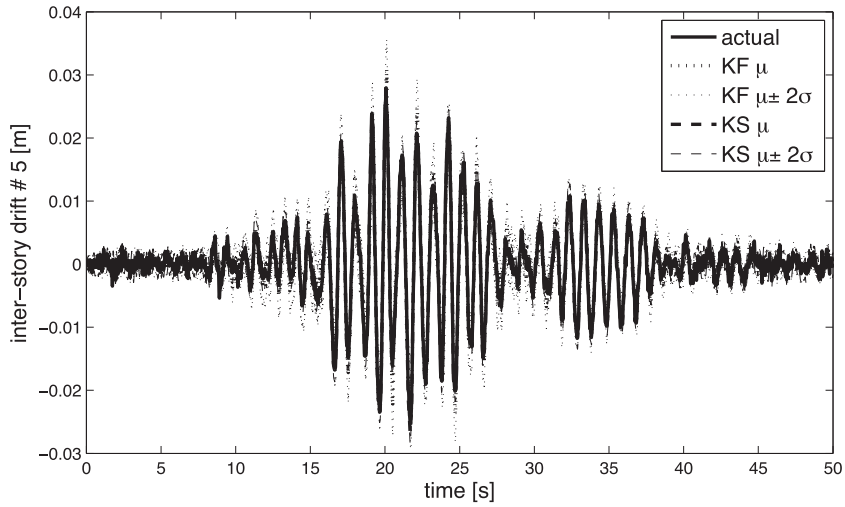


Fig. 6. Time history of inter-story drift #5: actual response, KF, and KS estimates.

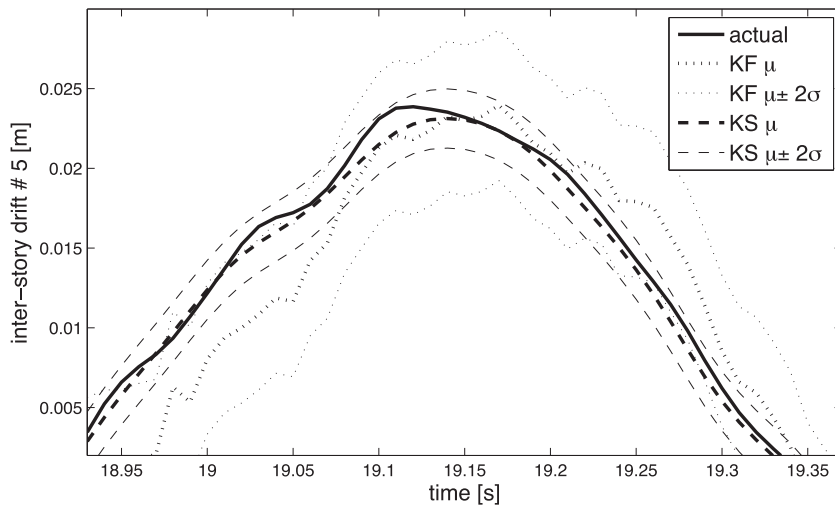


Fig. 7. Time history of inter-story drift #5: actual response, KF, and KS estimates (peak at $t = 19$ s).

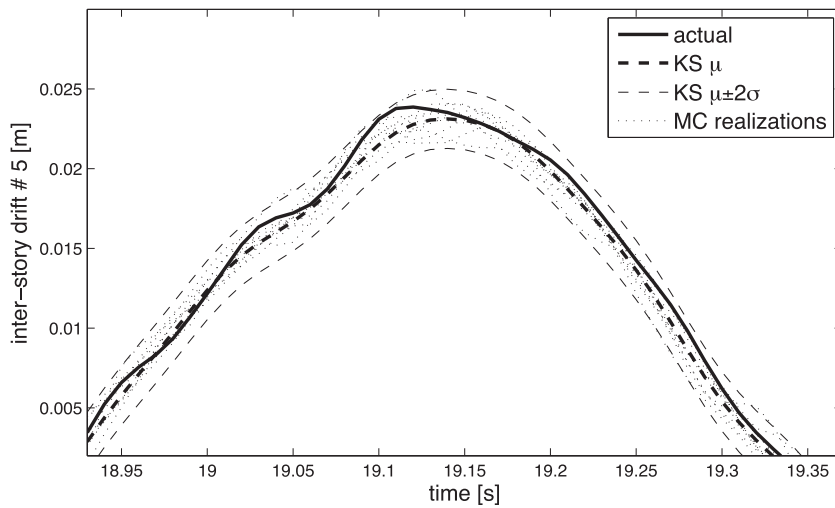


Fig. 8. MC realizations of inter-story drift #5 compared to actual response and KS estimate (peak at $t = 19$ s).

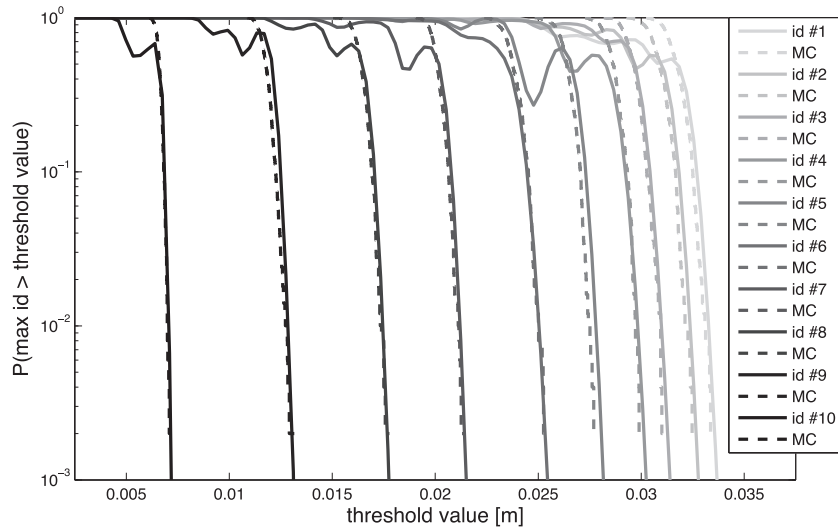


Fig. 9. Complementary CDF of maximum inter-story drift (“id”) from analytical solution and MC simulations.

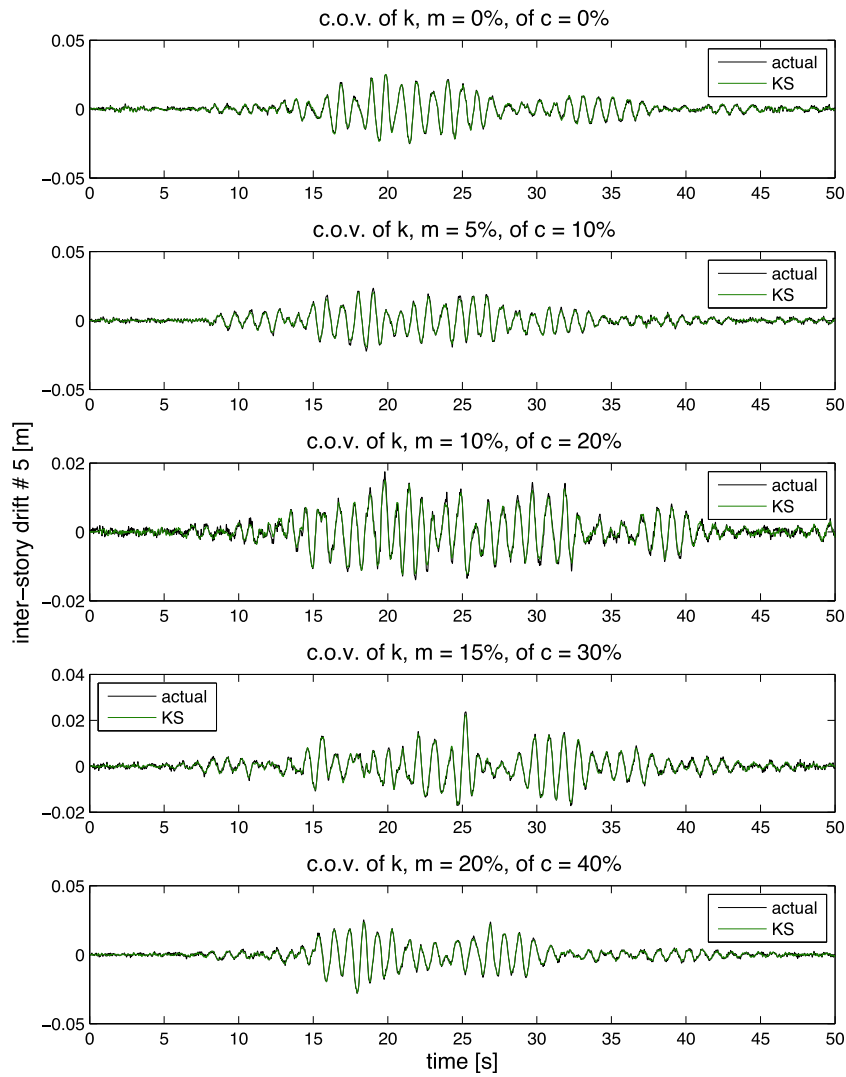


Fig. 10. Time history of inter-story drift #5: “actual” response versus mean KS estimates with varying c.o.v.’s of floor masses and story stiffnesses 0–20% and damping ratios 0–40%.

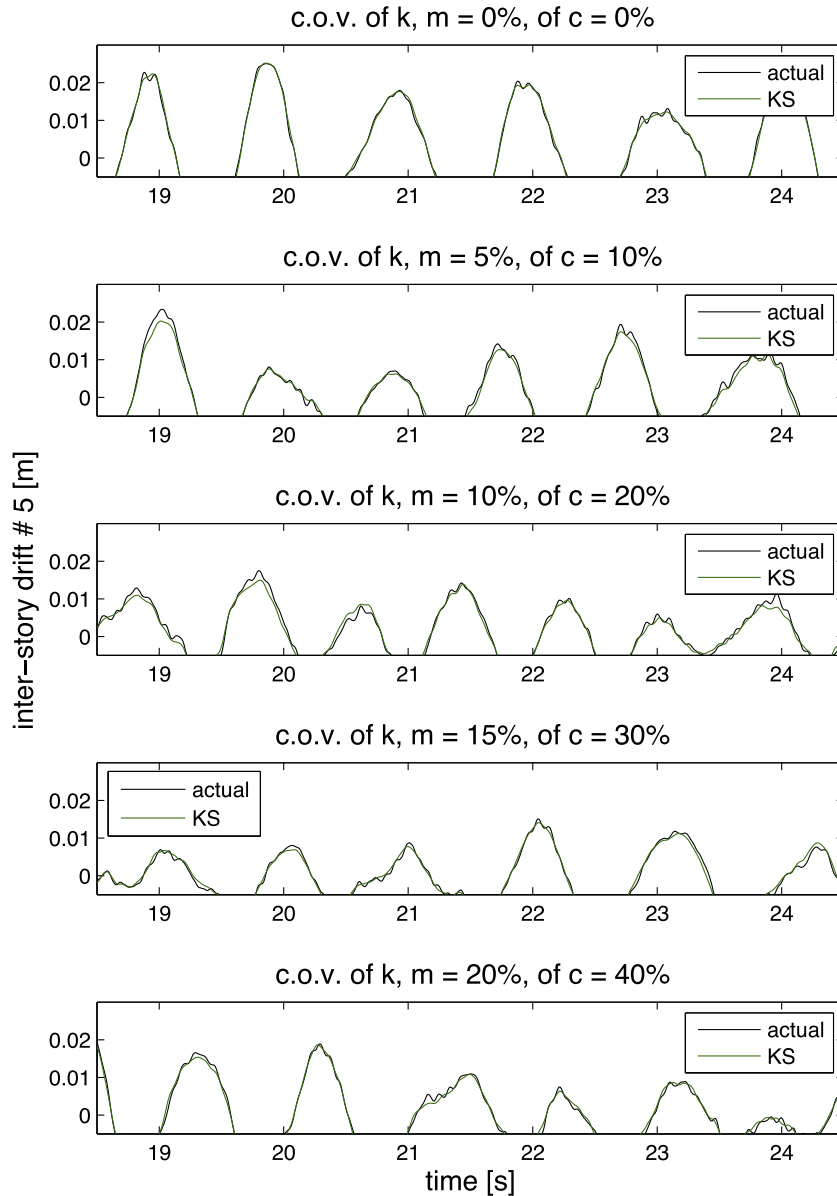


Fig. 11. Time history of inter-story drift #5: “actual” response versus mean KS estimates with varying c.o.v.’s of floor masses and story stiffnesses 0–20% and damping ratios 0–40% (peaks in interval $t = [19, 24]$ s).

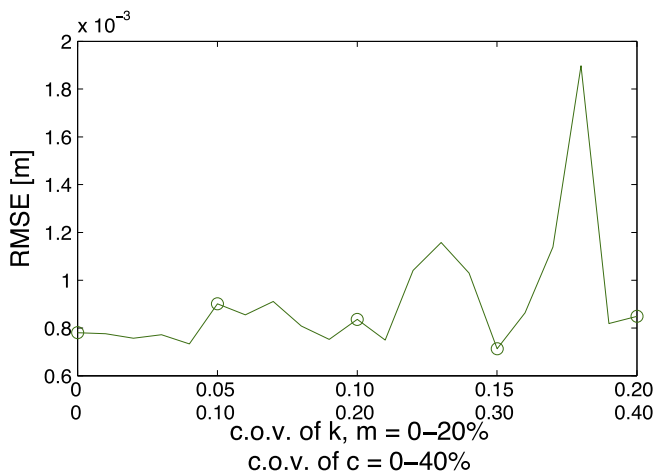


Fig. 12. RMSEs of mean KS-estimated inter-story drift #5 with varying c.o.v.’s of floor masses and story stiffnesses 0–20% and damping ratios 0–40%.

focus on the inter-story drift response, specifically that of the 5th story between floors 4 and 5. Thus, the proposed inference process enables us to estimate inter-story drift based on measured accelerations.

5.1. Estimates of the response

Previously, we investigated the impact of varying sensor noise, number, and placement on the estimation [32]. In that paper, we find that sensor placement has a more significant effect on the accuracy of the estimation than sensor precision. Sensors placed at the top of a structure are more informative than sensors placed at the bottom, and while increasing the precision of the sensors improves the estimation, the effect is small. Thus, for this study, we assume that one sensor is placed at the top floor of the building. We also assume the standard deviation of measurement error is $\sigma_v = 0.5 \text{ m/s}^2$.

Given this sensor configuration, Fig. 6 shows the time history of the inter-story drift #5. Plotted are the “actual” value, mean, and

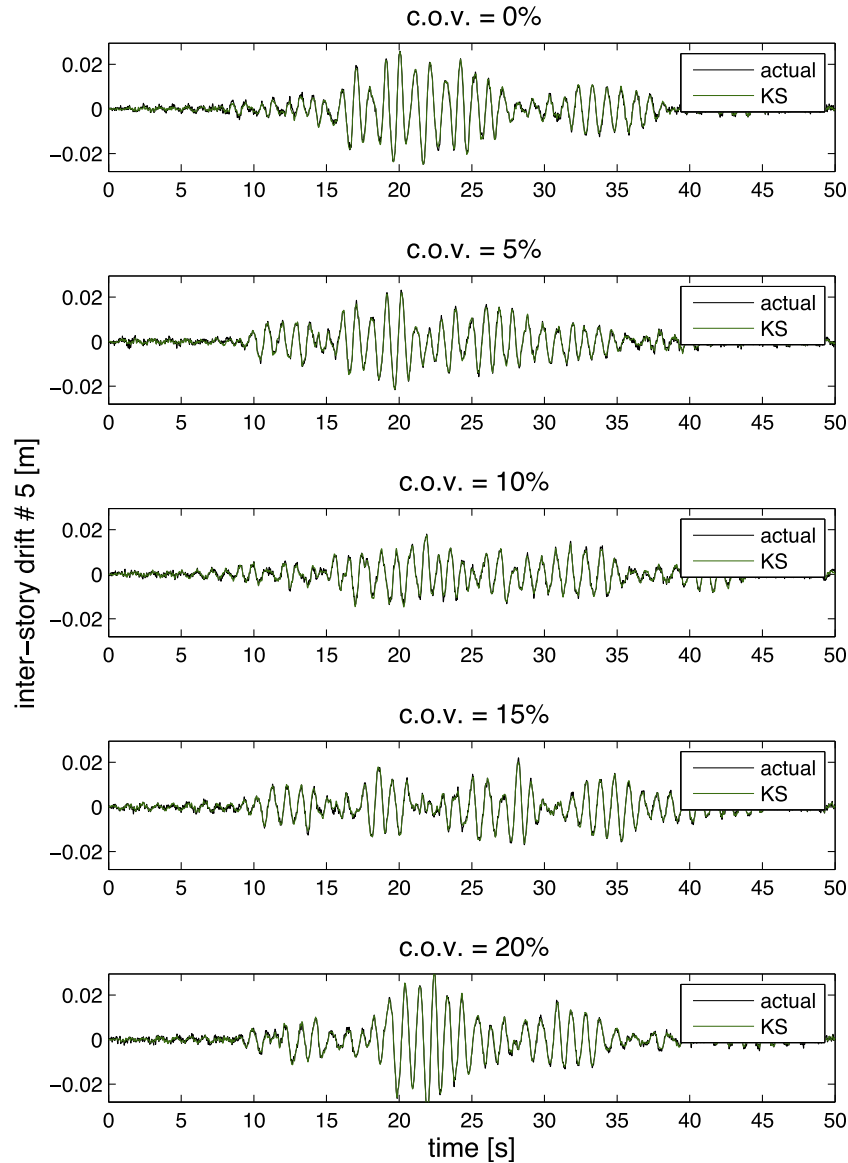


Fig. 13. Time history of inter-story drift #5: actual response versus mean KS estimates with varying c.o.v.'s of ground parameters 0–20%.

mean plus/minus two standard deviation values, representing the 95% confidence interval, of the KF and KS estimates. Because the time histories are nearly coinciding, Fig. 7 zooms on one particular peak that occurs at $t = 19$ s. Any other segment of the time history can similarly be chosen to analyze the results of the estimation. Comparing the actual response with the KF and KS estimates, we see that, consistent with the theory, employing the KS improves the accuracy of the estimation. Utilizing the measurement information over the entire time history results in a KS mean estimate that is closer to the actual inter-story drift and a decreased variance in the estimate. Hereafter, only the KS results are reported.

5.2. Distribution of maximum response

In analyzing the distribution of the maximum response, we compare the results we obtain from the analytical solution with those obtained from Monte Carlo (MC) simulations. For MC, we generate multiple realizations of the posterior process consistent with the inference on the DBN. Each MC realization produces a time history of the evolution of the structural response, including

the measurement noise. Sample trajectories are shown in Fig. 8 for 10 randomly selected realizations of inter-story drift #5, plus the “actual” value and the KS estimate. The segment of the time history around the peak at $t = 19$ s is selected.

In Fig. 8, we see that the MC realizations largely lie within the mean KS estimate of the response \pm two standard deviations. This represents the 95% confidence interval. Having these MC samples, we then take, for each realization, the maximum of the inter-story drift over the time period of analysis to obtain distributions of the maximum response.

The analytical solution derived in Section 4 gives us the probability that the maximum inter-story drift exceeded a given threshold, i.e., the complementary CDF. For comparison, we also compute these probabilities from the MC simulations. Fig. 9 shows the complementary CDF's of the inter-story drifts for all 10 stories obtained from the analytical solution versus MC. The analytical results (indicated by the solid lines) are obtained by using Eqs. (21) and (25). The MC results (indicated by the dotted lines) are the empirical CDF's. The MC solution employed 500 simulations. The lines shown are the mean estimates.

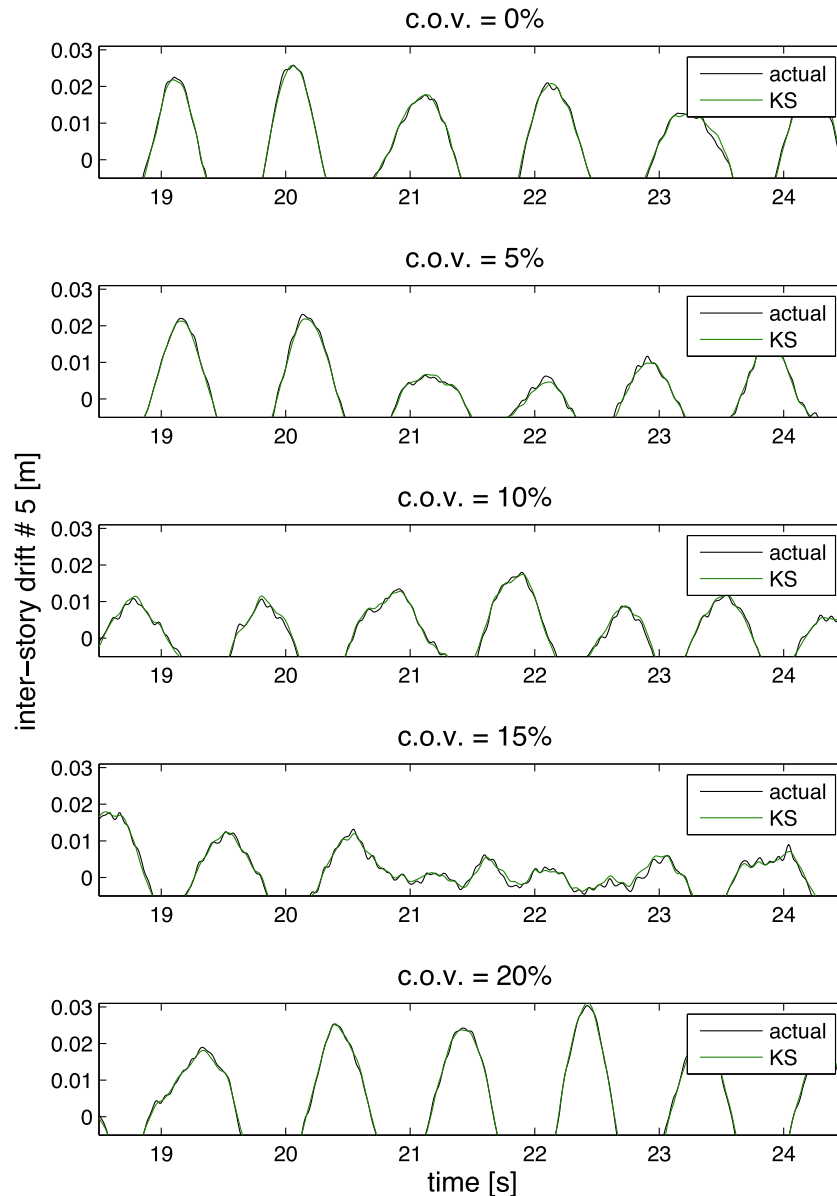


Fig. 14. Time history of inter-story drift #5: actual response versus mean KS estimates with varying c.o.v.'s of ground parameters 0–20% (peaks in interval $t = [19, 24]$ s).

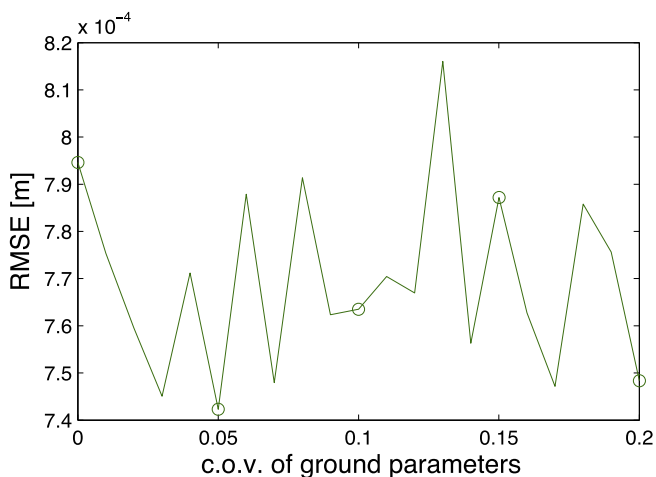


Fig. 15. RMSEs of mean KS-estimated inter-story drift #5 with varying c.o.v.'s of ground parameters 0–20%.

Examining the analytical results in Fig. 9, we see a phenomenon that cannot be true: For low thresholds, the complementary CDFs are not monotonically decreasing. This is due to the approximation employed in (21) for the distribution of the extreme value of a non-stationary process, namely the assumption that the threshold crossings constitute Poisson events. While this assumption is reasonable at high thresholds where crossings are rare, at low thresholds it is not good. One obvious reason is that the assumption does not account for the fact that once a threshold is crossed, the process cannot make additional crossings as long as it stays above that threshold. This “transition” time can be quite long for low thresholds. The comparison with MC results in Fig. 9 shows that the Poisson crossings assumption is valid for exceedance probabilities smaller than about 0.1. Since high thresholds are where damage occurs, this is indeed the range of interest for our analysis of the structural response. The advantage of the analytical solution, of course, is that it can provide solutions for much smaller exceedance probabilities for which the MC approach is infeasible.

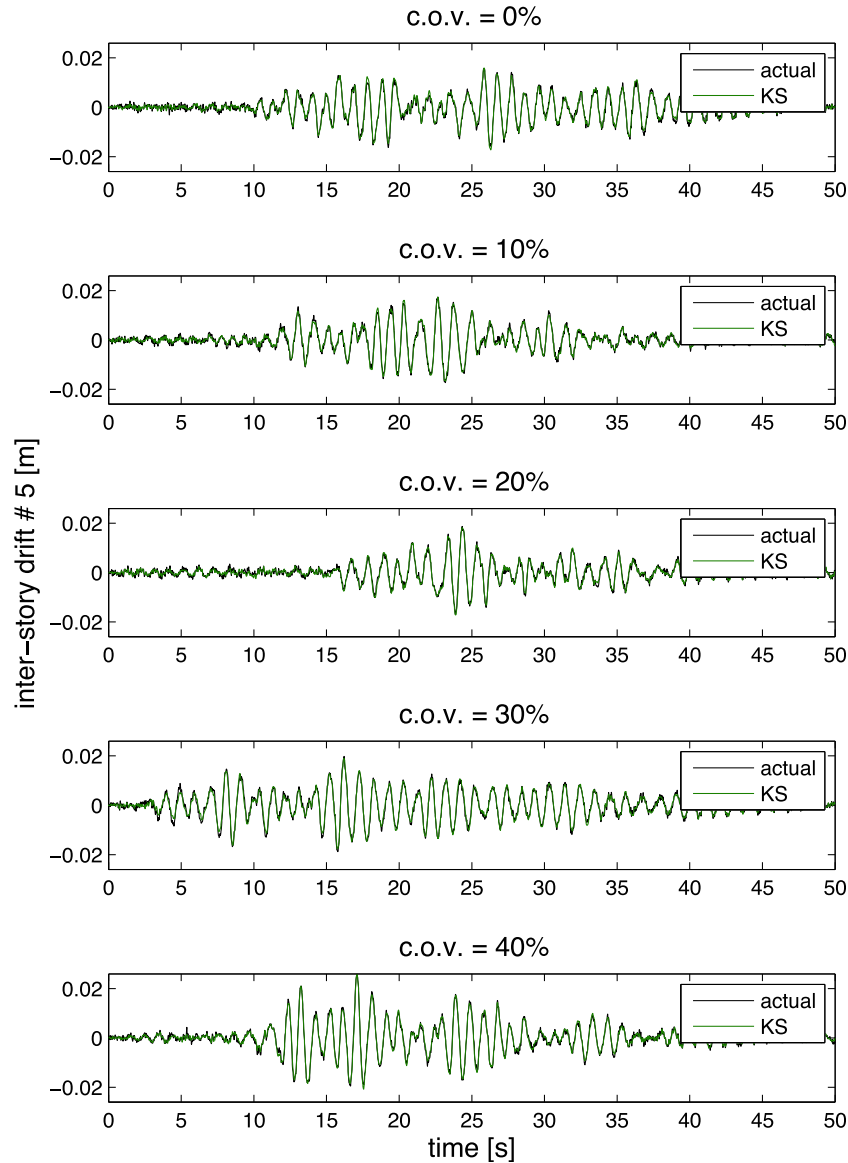


Fig. 16. Time history of inter-story drift #5: actual response versus mean KS estimates with varying c.o.v.'s of input motion parameters 0–40%.

5.3. Robustness to uncertainty in structural parameters

In the previous analyses, we assumed the parameters of the structure, i.e., mass, stiffness, damping, are known. In reality, these parameters are subject to uncertainty. In this section, we investigate the robustness of the estimation results to this uncertainty. We consider variability in all three parameters. More detailed results considering variability in subsets of the parameters are reported in [33].

In our analysis, we use nominal values of the structural parameters to obtain the KS estimates of the response. The nominal values represent our best estimates of the structural parameters based on design drawings. For the “actual” structure, the floor masses, story stiffnesses, and modal damping ratios are considered as random variables and vary from the nominal values. We sample the actual parameter values from lognormal distributions with means equal to the nominal value and over a range of coefficients of variation (c.o.v.'s), assuming statistical independence between floor masses, between story stiffnesses, and between modal

damping ratios. It is these randomly sampled values that we use in our simulation of the “actual” response and measured values.

Fig. 10 shows the effect of uncertainty in the structural parameters on the accuracy of the estimation of the inter-story drift #5 response over the full time history. The figure shows the “actual” response for a sampled set of structural parameters compared to the mean KS estimate as we increase the uncertainty in the parameters. The c.o.v. values for stiffness and mass range from 0% to 20% and that for damping ratios ranges from 0 to 40%. Since the curves in Fig. 10 are too close to be distinguished, Fig. 11 zooms on the peaks that occur in the interval $t \in [19, 24]$ s. Any other segment of the time history can similarly be chosen. For consistency and clarity, hereafter, we examine the peaks in this time segment.

In Figs. 10 and 11, because each level of c.o.v. corresponds to a random sample of the structural parameters that produces a different trajectory for the “actual” response, we compare each “actual” response with the corresponding mean KS estimate, as shown in each subplot. In the bottom subplot of Fig. 11, we see that even with all three structural parameters subject to the largest c.o.v.,

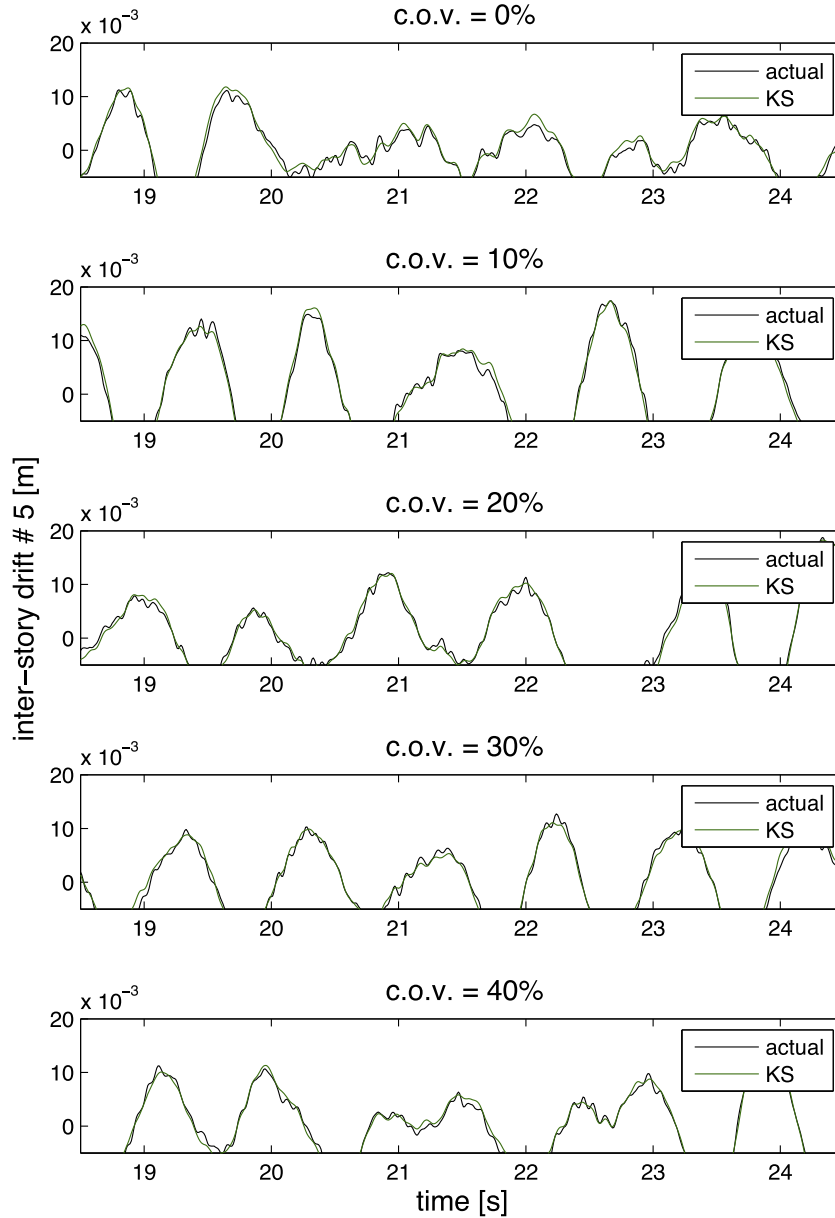


Fig. 17. Time history of inter-story drift #5: actual response versus mean KS estimates with varying c.o.v.'s of input motion parameters 0–40% (peaks in interval $t = [19, 24]$ s).

the mean KS estimate of the inter-story drift closely corresponds with the actual response.

To quantify the effect of uncertainty in the structural parameters on our inference results, we examine the root mean square errors (RMSEs) of the mean KS estimates of inter-story drift #5 compared to the actual responses as a function of the c.o.v.'s. The MSE is computed over the duration of the response $[0, 50]$ s as the average squared error between the estimated and actual inter-story drift values, and the RMSE is its square root. Fig. 12 shows the RMSEs computed across the range of c.o.v.'s with a step size of 0.01. The circles indicate the values at the five c.o.v. levels presented in Figs. 10 and 11. Note that the non-monotonicity of the RMSE is due to random variations, as the RMSE shown is the result from one simulation at each value of c.o.v.

In Fig. 12, we see that, as expected, the RMSE increases with increasing uncertainty in the structural parameters. The increase, however, is gradual and relatively small in magnitude. Specifically, the RMSE increases from 7.8×10^{-4} m to 8.5×10^{-4} m (a 10%

increase) with a maximum of 1.9×10^{-3} m over c.o.v. values ranging from 0–20% for floor masses and story stiffnesses and 0–40% for damping ratios. The maximum RMSE is an order of magnitude smaller than the actual peak inter-story drift response in each case.

The reason the inference is robust relative to the uncertainty in the structural parameters is due to the updating that is performed with the formulation of the problem. The variability in the structural parameters affects the estimate of the system state. However, at each time step, we have information from the sensor measurements, and we use this information to update the estimation. This updating occurs at every time step, in this case $\Delta t = 0.01$ s. Thus, the estimate is quickly corrected by the measurement information before the estimate has time to evolve incorrectly based on the incorrectly assumed nominal values of structural parameters in the estimation equations.

In looking at inter-story drift, another possible explanation for the robustness of the results to uncertainty in the structural parameters is that there may be a cancellation of errors that occurs

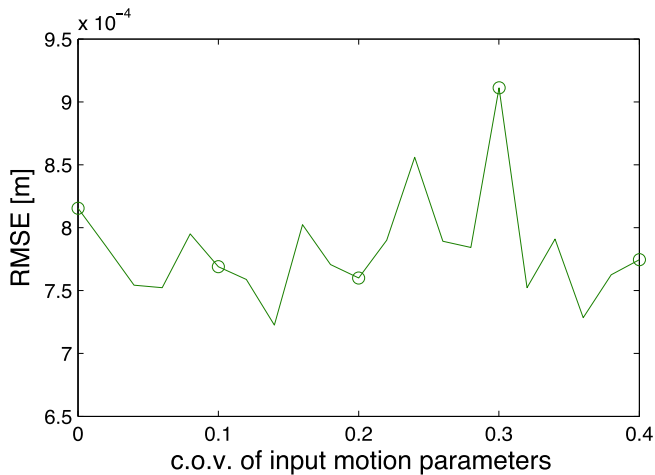


Fig. 18. RMSEs of KS-estimated inter-story drift #5 with varying c.o.v.'s of input motion parameters 0–40%.

when subtracting displacements of adjacent floors to compute the inter-story drift. To ensure that the accuracy of the estimation is not due to this cancellation, we also investigated the results in estimating individual floor displacements. The results of this analysis, not shown here, showed similar robustness to parameter uncertainties. Thus, the proposed method is able to estimate the state of the considered structural system accurately, even when all three structural parameters – mass, stiffness, and damping – are subject to uncertainty.

5.4. Robustness to uncertainty in ground parameters

Next, we investigate the robustness of the inference results to uncertainty in the ground parameters. The nominal values of the ground parameters are set to $\omega_g/2\pi = 1.5$ Hz and $\xi_g = 0.4$. These represent our best guess of the soil characteristics and are the values we use in our estimation of the system state. The “actual” parameter values are randomly sampled from the lognormal distribution with the mean equal to the nominal value and over a range of c.o.v.'s from 0% to 20%. Fig. 13 shows the full time history of the actual and estimated mean KS inter-story drift #5 response. Fig. 14 shows the results for the peaks that occur in the time segment $t \in [19, 24]$ s.

In Figs. 13 and 14, we see that varying the ground parameters produces varying structural response trajectories. However, in each case, the mean KS estimate is close to the actual response. Despite the variation in the ground parameters and response trajectories, the estimation performs well. Fig. 15 shows the RMSEs of the mean KS estimates of inter-story drift #5 computed over the duration of the response as a function of the c.o.v. It is observed that the accuracy of the estimation is insensitive to the degree of uncertainty in the ground parameters, as the RMSE remains essentially constant with a mean of 7.7×10^{-4} over the range of c.o.v.'s from 0% to 20%. The maximum value of the RMSE is around 10% of the maximum actual inter-story drift.

5.5. Robustness to uncertainty in input motion parameters

Finally, we investigate the robustness of the proposed method to uncertainty in the input motion parameters. We vary the descriptive variables of the seismic event, i.e., the time of the maximum intensity of the ground motion, t_{eq}^{max} , and the effective duration of the earthquake motion, D_{5-95} . In addition, we vary the scale factor of the gamma modulating function, i.e., to randomize the

intensity of the ground motion. We assume the nominal values $t_{eq}^{max} = 20$ s, $D_{5-95} = 25$ s, and a scale factor of 200 in our estimation of the system state. We then randomly sample realizations of these parameters from lognormal distributions with means equal to the nominal values and c.o.v.'s ranging from 0% to 40%. The sampled values are then used to simulate the “actual” ground motion. Fig. 16 shows the full time history of the “actual” and mean KS-estimated inter-story drift #5 response. Fig. 17 shows the results for the peaks that occur in the time segment $t \in [19, 24]$ s. We see in these figures that, in each case, the mean KS estimate of the response is close to the “actual” response, and the estimation performs well across time histories. Fig. 18 shows the RMSEs of the mean KS estimates of inter-story drift #5 computed over the duration of the response as a function of c.o.v. It is observed that the variability in the RMSE of the estimate increases slightly with increasing c.o.v. of the input ground motion parameters. The value of the RMSE, however, remains essentially constant over the range of c.o.v.'s 0–40% with a mean of 7.9×10^{-4} m. The maximum RMSE is more than an order of magnitude smaller than the actual peak inter-story drift response.

In summary, while in general model errors can significantly deteriorate the accuracy of the inference, we conjecture that low sensitivity to errors in the model parameters holds for applications similar to that investigated in this example.

6. Conclusions

We have presented a probabilistic framework for estimating the state of a linear system subject to stochastic excitation based on uncertain sensor measurements. We have shown the methodology to be able to accurately perform inference on the dynamically evolving response of a structure under earthquake load based on accelerometer data. In addition, we have presented an analytical solution to obtain the distribution of the peak response over the duration of the excitation.

The proposed framework is applied to the estimation of the maximum inter-story drift in a multi-story shear-type building. By allowing the system parameters to vary randomly, we have shown the methodology to be robust to uncertainties in the structural, ground, as well as input motion characteristics, demonstrating the ability of the proposed method to perform accurate estimation of the response even under conditions of parameter uncertainties.

Acknowledgments

The first author acknowledges support from the National Science Foundation Graduate Research Fellowship. Additional support was provided by the National Science Foundation Grant No. CMMI-1130061, which is also gratefully acknowledged.

References

- [1] Kalman RE. A new approach to linear filtering and prediction problems. *J Basic Eng* 1960;82(1):35–45.
- [2] Rauch HE, Tung F, Striebel CT. Maximum likelihood estimates of linear dynamic systems. *AIAA J* 1965;3(8):1445–50.
- [3] Simon D. Optimal state estimation: Kalman, H infinity, and nonlinear approaches. 1st ed. Hoboken, NJ: Wiley; 2006.
- [4] Murphy K. Machine learning: a probabilistic perspective. Boston: MIT Press; 2012.
- [5] Dean T, Kanazawa K. A model for reasoning about persistence and causation. *Comput Intell* 1989;5(3):142–50.
- [6] Hoshiya M, Saito E. Structural identification by extended Kalman filter. *J Eng Mech* 1984;110(12):1757–70.
- [7] Yang JN, Lin S, Huang H, Zhou L. An adaptive extended Kalman filter for structural damage identification. *Struct Control Health Monitor* 2006;13(4):849–67.

- [8] Wu M, Smyth AW. Application of the unscented Kalman filter for real-time nonlinear structural system identification. *Struct Control Health Monitor* 2007;14:971–90.
- [9] Yuen KV, Katafygiotis LS. Bayesian modal updating using complete input and incomplete response noisy measurements. *J Eng Mech* 2002;128(3):340–50.
- [10] Au SK, Zhang FL, Ni YC. Bayesian operational modal analysis: theory, computation, practice. *Comput Struct* 2013;126:3–14.
- [11] Katafygiotis LS, Yuen KV. Bayesian spectral density approach for modal updating using ambient data. *Earthquake Eng Struct Dynam* 2001;30(8):1103–23.
- [12] Vanik MW, Beck JL. A Bayesian probabilistic approach to structural health monitoring. In: *Proceedings of the International Workshop on structural health monitoring*. p. 140–51 [Lancaster, PA].
- [13] Vanik MW, Beck JL, Au SK. Bayesian probabilistic approach to structural health monitoring. *J Eng Mech* 2000;126(7):738–45.
- [14] Straser EG, Kiremidjian AS. Monitoring and evaluating civil structures using measured vibration. *Proc SPIE* 1996;2719:112–22.
- [15] Kottapalli VA, Kiremidjian AS, Lynch JP, Carryer E, Kenny TW, Law KH, et al. Two-tiered wireless sensor network architecture for structural health monitoring. *Proc SPIE* 2003;5057:8–19.
- [16] Wu S, Beck JL. Synergistic combination of systems for structural health monitoring and earthquake early warning for structural health prognosis and diagnosis. *Proc SPIE* 2012;8348.
- [17] Gasparini DA, Tsiatas G, Sun WJ, Shah A, Shein SL. Random vibration of cascaded secondary system. In: *Proceedings of the 7th SMIRT Conference*. p. 445–51 [Chicago, Illinois].
- [18] Johansson R, Verhaegen M, Chou CT. Stochastic theory of continuous-time state-space identification. *IEEE Trans Signal Process* 1999;47(1):41–51.
- [19] Rezaeian S, Der Kiureghian A. Stochastic modeling and simulation of ground motions for performance-based earthquake engineering. Pacific Earthquake Engineering Research Center (PEER) Report No. 2010/02. Berkeley: University of California; 2010.
- [20] Oppenheim AV, Schaffer RW, Buck JR. *Discrete-time signal processing*. 3rd ed. Upper Saddle River, NJ: Prentice-Hall; 2009.
- [21] Meinhold RJ, Singpurwalla ND. Understanding the Kalman filter. *Am Statistician* 1983;37(2):123–7.
- [22] Hamilton JD. *Time series analysis*. New Jersey: Princeton University Press; 1994.
- [23] West M, Harrison J. *Bayesian forecasting and dynamic models*. 2nd ed. Springer Series in Statistics; 1999.
- [24] Doucet A, de Freitas N, Murphy K, Russell S. Rao-Blackwellised particle filtering for dynamic Bayesian networks. *Proceedings of the 16th Conference on Uncertainty in Artificial Intelligence*. p. 176–83.
- [25] Chen Z. Bayesian filtering: from Kalman filters to particle filters, and beyond. *Statistics* 2003;182(1):1–69.
- [26] Antsaklis PJ, Michel AN. *A linear systems primer*. Boston: Birkhauser; 2007.
- [27] Welch G, Bishop G. An introduction to the Kalman filter, Technical Report 95-041. Department of Computer Science, University of North Carolina at Chapel Hill; 1995.
- [28] Murphy KP. *Dynamic Bayesian Networks: representation, inference and learning* [Doctoral thesis]. Berkeley: University of California; 2002.
- [29] Barber D. *Bayesian reasoning and machine learning*. Cambridge: Cambridge University Press; 2012.
- [30] Lutes L, Sarkani S. *Random vibrations: analysis of structural and mechanical systems*. Burlington, MA: Elsevier; 2004.
- [31] Rice SO. Mathematical analysis of random noise. *Bell Syst Tech J* 1944;23(3):282–332.
- [32] Tien I, Pozzi M, Der Kiureghian A. Inference on maximum structural response based on measured accelerations using dynamic Bayesian network. In: Deodatis G, Ellingwood B, Frangopol D, editors. *Safety, reliability, risk and life-cycle performance of structures and infrastructures*. New York: CRC Press; 2013. p. 2481–8.
- [33] Tien I. *Bayesian network methods for modeling and reliability assessment of infrastructure systems* [Doctoral thesis]. Berkeley: University of California; 2014.